Reducing Localization Error of Vision-Guided Industrial Robots

Marek Franaszek
National Institute of Standards and Technology
Gaithersburg, MD 20899 USA
marek@nist.gov

Geraldine S. Cheok
National Institute of Standards and Technology
Gaithersburg, MD 20899 USA
cheok@nist.gov

Jeremy A. Marvel
National Institute of Standards and Technology
Gaithersburg, MD 20899 USA
jeremy.marvel@nist.gov

***Abstract*—In many manufacturing applications, such as automated drilling or inspection of large parts, accurate knowledge of both position and orientation of the robot end-effector is critical. In this paper, a method for reducing robot end-effector position and orientation error is presented. Experimental results show that the method can reduce the median position error by 97% (to 0.3 mm) and the median orientation error by 57% (to 0.27 deg). Limitations of the method caused by the hand-eye calibration are discussed.**

Keywords—robot localization error, hand-eye calibration, rigid-body registration, volumetric error compensation, accuracy, repeatability

I. INTRODUCTION

Industrial robots are known for their good repeatability, often to within tens of microns. At the same time, their accuracy may frequently exceed millimeters [1, 2]. This lack of accuracy seriously limits the use of these robots in performing manufacturing tasks which require accurate localization of the end-effector. For example, a robot arm with large localization error tasked with part assembly will result in frequent jamming [3]. Automated drilling [4] or welding [5] require accurate knowledge of the Tool Center Point (TCP) frame. Inspections of large parts [6, 7] (e.g., wind turbine blades [8] or airplane components [9]) performed with line-of-sight sensors (e.g., laser scanners) mounted on a robot arm require the registration of scans acquired from different poses so that the differences between the as-built part and the original model design can be determined. This requires very accurate location of the sensor frame at the different poses. Thus, reducing robot localization error is an important research subject with immediate practical implications.

The industrial robot spatial error can be traced back to two root causes: 1) incorrect values of the Denavit-Hartenberg (DH) parameters in the robot arm kinematic model, and 2) other, non-kinematic errors such as thermal effects, backlash, friction, drift, joint compliance, or deformation under gravity load which especially affect light weight robots. The first source of error is caused mainly by incorrect or imprecise values of the joint-offsets, and it is responsible for roughly 80% of the total robot localization error [10, 11]. This kind of error can be reduced by remastering the robot for which many different calibration techniques have been developed [12-14]. However, the residual error remains even after remastering, and it affects robot performance. The remaining part of the total robot localization error can be attributed to non-kinematic errors which are difficult to model and hard to reduce.

To compensate for the robot localization error, different solutions have been proposed which depend on the specifics of a particular task. For example, video servoing [15, 16] can decrease robot error to a level comparable to the accuracy of a visual sensor, but it requires constant tracking of the robot end effector relative to a target point which may be difficult in some applications (e.g., medical surgery). For part assembly, a frequently used strategy relies on active compliance control based on feedback from force/torque (F/T) sensors. Many different control strategies have been developed and their performance evaluated in different versions of the peg-in-hole test [17-20]. For different manufacturing tasks, such as part inspection performed by non-contact sensors [21, 22], feedback from F/T sensors is not available and other solutions had to be developed. These rely on external visual sensors and analytical models of error to provide small corrections to the commanded robot pose. Such Volumetric Error Compensation (VEC) techniques [23-29] require knowledge of the rigid-body transformation (i.e., rotation matrix $\boldsymbol{\Omega}$ and translation vector $\boldsymbol{\tau}$) between the robot frame and the external sensor frame.

To register the sensor frame to the robot frame, the locations of a set of three or more points must be known in both frames. Once the points are measured in three-dimensional (3D) Cartesian space, the transformation $\{\boldsymbol{\Omega}, \boldsymbol{\tau}\}$ can be calculated [30]. Once the transformation is known, it can be used to transform any point from the sensor frame to the robot frame. However, due to robot localization error, the rigid-body condition is not preserved, and the transformed point in the sensor frame is not mapped exactly onto the corresponding point in the robot frame. In [31], a procedure called the Restoration of Rigid Body Condition (RRBC) was developed: its application allowed reduction of mean robot positional error by more than 90% (up to 0.15 mm). The original RRBC used point-based registration and could lead to reduction in positional error only. However, in applications such as automated drilling [4] or part inspection [22], not only is point location important but the

orientation of the TCP frame is also critical. Furthermore, the location of a point in the robot frame cannot always be determined from forward kinematics alone because of the unknown offset transformation between the robot wrist frame and the TCP frame. In these cases, point-based registration cannot be performed, and hand-eye (robot-sensor) calibration must be used instead [32]. This requires measurement of the full pose, i.e., six degrees of freedom (6DOF) data.

In this paper, we extend the original RRBC procedure to handle this more general case. Experiments show that the median orientation error was reduced by 57% while the median positional error was reduced by 97%.

II. Related work

The use of the VEC type methods to reduce localization error requires prior knowledge of the transformation between two coordinate frames: the robot frame $\{\boldsymbol{A}\}$, and the sensor frame $\{\boldsymbol{B}\}$. When the tracking system can only measure 3D points, the transformation $\{\boldsymbol{\Omega}, \boldsymbol{\tau}\}$ can be obtained by minimizing the following error function $FRE(\boldsymbol{\Omega}, \boldsymbol{\tau})$ [30] for a set of J points:

$$FRE(\boldsymbol{\Omega}, \boldsymbol{\tau}) = \frac{1}{J}\sum_{j=1}^{J} \boldsymbol{\varepsilon}_j^2, \tag{1}$$

where $\boldsymbol{\varepsilon}_j$ is a small error vector calculated as

$$\boldsymbol{\varepsilon}_j = \boldsymbol{\Omega}\boldsymbol{b}_j + \boldsymbol{\tau} - \boldsymbol{a}_j\,, \tag{2}$$

and $\boldsymbol{a}_j, \boldsymbol{b}_j$ are locations of the j-th 3D point in the corresponding frames. Points for registration are selected from a larger set of common points measured in both frames, which we call fiducials. A non-zero residual value of FRE means that the rigid-body condition is not satisfied and $\|\boldsymbol{a}_i - \boldsymbol{a}_j\| \neq \|\boldsymbol{b}_i - \boldsymbol{b}_j\|$ for most $i, j \leq J$, where $\|\ldots\|$ is the Euclidean distance. Once $\{\boldsymbol{\Omega}, \boldsymbol{\tau}\}$ is determined, any point $\boldsymbol{\beta}$ measured in sensor frame $\{\boldsymbol{B}\}$ can be transformed to a point $\tilde{\boldsymbol{\alpha}}$ in the robot frame $\{\boldsymbol{A}\}$

$$\tilde{\boldsymbol{\alpha}} = \boldsymbol{\Omega}\,\boldsymbol{\beta} + \boldsymbol{\tau}\,. \tag{3}$$

If a point $\boldsymbol{\alpha}$ (corresponding to point $\boldsymbol{\beta}$) is not measured in the robot frame, the small correction error defined in (2) cannot be calculated. Rather, it can only by approximated from nearby fiducials as

$$\boldsymbol{\varepsilon}_\alpha = \sum_{j=1}^{J} w_j(\tilde{\boldsymbol{\alpha}})\,\boldsymbol{\varepsilon}_j, \tag{4}$$

where w_j are normalized weights such that $\sum_{j=1}^{J} w_j = 1$. Point $\boldsymbol{\beta}$, measured only in the sensor frame $\{\boldsymbol{B}\}$ but required in the robot frame $\{\boldsymbol{A}\}$, is called a target. The approximated error (4) can be used as a correction to the transformed target (3) so that the corrected target $\tilde{\boldsymbol{\alpha}} + \boldsymbol{\varepsilon}_\alpha$ is supposedly closer to the true, unknown target location $\boldsymbol{\alpha}$ in the robot frame $\{\boldsymbol{A}\}$. In this study, targets are also measured in the robot frame, and the target error $\delta(\boldsymbol{\alpha})$, calculated as

$$\delta(\tilde{\boldsymbol{\alpha}}) = \|\boldsymbol{\Omega}\,\boldsymbol{\beta} + \boldsymbol{\tau} + \boldsymbol{\varepsilon}_\alpha - \boldsymbol{\alpha}\|, \tag{5}$$

can be used to gauge the reduction in the robot position error.

Different VEC algorithms calculate statistical weights w_j in (4) differently. Recently, a kriging procedure, commonly used in geostatistics [33], was applied to decrease the positional error of an aviation drilling robot from 1.393 mm to 0.106 mm [34]. A similar approach was applied to a drilling and riveting system, and it resulted in a reduction of the localization error from 2.01 mm to 0.32 mm [35]. Calculations of weights w_j in (4) were based on an error similarity concept (similar configurations of robot joint angles should result in similar robot positioning error) and were derived from experimentally determined semi-variograms [36]. In both studies [34, 35], a laser tracker and a spherically mounted reflector (SMR) were used to track the robot movement and calculate $\boldsymbol{\varepsilon}_j$ fiducial errors at $J = 200$ locations. Then, the weights w_j in (4) were calculated for another set of target points, the estimated correction (4) was evaluated at each target, and the target positional error (5) was used to gauge the reduction of the robot error. Neither orientation errors for fiducials nor estimated orientation corrections for targets were calculated in either study.

A different method based on fuzzy interpolation was developed and tested using simulation [37]. The kinematic model of the robot with known parameters was used to generate ground truth of a robot pose (thus, no registration between two coordinate frames was needed), and the position of the end-effector was perturbed by noise to simulate experimental conditions. Fiducials were distributed on a regular grid, and the corrections to target positions were interpolated from the eight nearest surrounding fiducial errors. The weights w_j in (4) were derived from fuzzy inference and provided better reduction in target error (5) when compared with the usual three-linear interpolation scheme. The fuzzy scheme was later extended to the three orientation angles which were formally treated in the calculations in the same way as the three Cartesian components of position vector [38]. Fuzzy interpolation from [37] was also used in [34] on experimental data, but yielded larger target positional error than the original method based on kriging.

The approaches described above do not rely on robot calibration nor analytical error models. Instead, a robot is dynamically tracked by an external vision system and small corrections to the commanded positions are continuously provided to the robot controller. In this paper, we present an extension of the RRBC method (which also does not require the development of an error model) to compensate for the position as well as orientation errors. The results from experiments requiring full hand-eye calibration are presented. Comparison with simulation results reveals why the reduction of positional error is much better than reduction of orientation error.

III. Extension of RRBC method

In the more general case when there is a constant offset transformation $\widehat{\boldsymbol{X}}$ between the TCP frame and the frame associated with the end of the robot arm, hand-eye calibration is needed to find the transformation $\widehat{\boldsymbol{Y}}$ from the sensor frame to the robot frame. This procedure requires $J \geq 3$ different measurements of corresponding poses $\widehat{\boldsymbol{B}}_j$ in the sensor frame and $\widehat{\boldsymbol{A}}_j$ in the robot frame. Both homogeneous transformations can be calculated by solving the set of equations

$$\widehat{\boldsymbol{A}}_j\,\widehat{\boldsymbol{X}} = \widehat{\boldsymbol{Y}}\,\widehat{\boldsymbol{B}}_j \tag{6}$$

for all $j = 1, \ldots, J$. Equation (6) can be rewritten for the orientation and the position part separately as

$$\boldsymbol{A}_j\,\boldsymbol{X} = \boldsymbol{Y}\,\boldsymbol{B}_j\,, \tag{7a}$$

$$\boldsymbol{A}_j\,\boldsymbol{x} + \boldsymbol{a}_j = \boldsymbol{Y}\,\boldsymbol{b}_j + \boldsymbol{y}\,, \tag{7b}$$

where $\boldsymbol{X}, \boldsymbol{Y}, \boldsymbol{A}_j, \boldsymbol{B}_j$ are 3×3 rotation matrices and $\boldsymbol{x}, \boldsymbol{y}, \boldsymbol{a}_j, \boldsymbol{b}_j$ are column vectors. There are many different methods to solve (7) for $\widehat{\boldsymbol{X}}$ and $\widehat{\boldsymbol{Y}}$. In this study, we used a modified analytical solution based on the Kronecker product developed in [39]. The original method does not guarantee that matrices $\boldsymbol{X}$ and $\boldsymbol{Y}$ are orthogonal, and therefore, we apply an orthogonalization procedure to the resulting matrices as described in [40]. After the homogeneous matrices $\widehat{\boldsymbol{X}}$ and $\widehat{\boldsymbol{Y}}$are determined, poses from the sensor frame $\{\boldsymbol{B}\}$ can be transformed to the robot frame $\{\boldsymbol{A}\}$. As in the point-based, rigid-body registration, poses mapped from the sensor frame do not exactly match the corresponding measured poses in the robot frame. Analogous to the vector error $\boldsymbol{\varepsilon}_j$ in (2), a small rotation matrix $\boldsymbol{\Lambda}_j$ and a position vector $\boldsymbol{\lambda}_j$ are calculated from (7) as

$$\boldsymbol{\Lambda}_j = \boldsymbol{Y}\,\boldsymbol{B}_j\,\boldsymbol{X}^T\,\boldsymbol{A}_j^T\,, \tag{8a}$$

$$\boldsymbol{\lambda}_j = \boldsymbol{Y}\,\boldsymbol{b}_j + \boldsymbol{y} - \left(\boldsymbol{A}_j\,\boldsymbol{x} + \boldsymbol{a}_j\right), \tag{8b}$$

where $\boldsymbol{X}^T$ indicates a transposed matrix. Once matrices $\boldsymbol{\Lambda}_j$ and vectors $\boldsymbol{\lambda}_j$ are calculated from fiducial poses $\widehat{\boldsymbol{A}}_j$ and $\widehat{\boldsymbol{B}}_j$, they can be used to estimate the orientation and position corrections of a target pose $\left(\widetilde{\mathbf{A}}, \widetilde{\boldsymbol{\alpha}}\right)$ transformed to the robot frame from the sensor frame

$$\boldsymbol{\Lambda}_a\left(\widetilde{\mathbf{A}},\ \widetilde{\boldsymbol{\alpha}}\right) = ort\left(\textstyle\sum_{j=1}^{J} w_j\,\boldsymbol{\Lambda}_j\right), \tag{9a}$$

$$\boldsymbol{\lambda}_a\left(\widetilde{\mathbf{A}},\ \widetilde{\boldsymbol{\alpha}}\right) = \textstyle\sum_{j=1}^{J} w_j\,\boldsymbol{\lambda}_j\,, \tag{9b}$$

where $ort(\ldots)$ denotes the orthogonalization procedure developed in [40], and $\left(\widetilde{\mathbf{A}}, \widetilde{\boldsymbol{\alpha}}\right)$ is the target pose $(\mathbf{B}, \boldsymbol{\beta})$ transformed from the sensor frame to the robot frame using

$$\widetilde{\mathbf{A}} = \boldsymbol{Y}\,\mathbf{B}\,\boldsymbol{X}^T\,, \tag{10a}$$

$$\widetilde{\boldsymbol{\alpha}} = \boldsymbol{Y}\,\boldsymbol{\beta} + \boldsymbol{y} - \widetilde{\mathbf{A}}\,\boldsymbol{x}. \tag{10b}$$

The corrected target rotation $\boldsymbol{\Lambda}_a\widetilde{\mathbf{A}}$ and the corrected target position $\widetilde{\boldsymbol{\alpha}} + \boldsymbol{\lambda}_a$ should be closer to the actual (and usually unknown) rotation $\mathbf{A}$ and position $\boldsymbol{\alpha}$ in the robot frame. Again, as in (5), when the target pose $(\mathbf{A}, \boldsymbol{\alpha})$ is also measured in the robot frame, the corresponding target error can be calculated and used to gauge the performance of the error compensation procedure.

For the orientation error, we rely on the angle-axis $(\rho, \boldsymbol{u})$ representation of the rotation $\boldsymbol{R}(\rho, \boldsymbol{u})$, and the fact that angle ρ is invariant to the coordinate system (i.e., it is analogous to vector length). We ensure that ρ is always non-negative by using the property of rotation that $\boldsymbol{R}(-\rho, \boldsymbol{u}) = \boldsymbol{R}(\rho, -\boldsymbol{u})$. Thus, the target error has two components (ρ, δ), and they were evaluated for the uncorrected poses in robot frame using

$$\boldsymbol{R}(\rho_{unc}, \boldsymbol{u}_{unc}) = \widetilde{\mathbf{A}}\,\mathbf{A}^T\,, \tag{11a}$$

$$\delta_{unc} = \|\widetilde{\boldsymbol{\alpha}} - \boldsymbol{\alpha}\|\,, \tag{11b}$$

as well as for the corrected poses using

$$\boldsymbol{R}(\rho_{cor}, \boldsymbol{u}_{cor}) = \boldsymbol{\Lambda}_a\widetilde{\mathbf{A}}\,\mathbf{A}^T\,, \tag{12a}$$

$$\delta_{cor} = \|\widetilde{\boldsymbol{\alpha}} + \boldsymbol{\lambda}_a - \boldsymbol{\alpha}\|\,. \tag{12b}$$

The weights, w_j, were those used to calculate the orientation corrections in (9a) and position correction in (9b). We calculated the Euclidean distances d_j between the joint angles of the robot arm $\{\theta_t\}$ corresponding to the target pose, and the joint angles of the j-th fiducial $\{\theta_{f,j}\}$

$$d_j = \sqrt{\textstyle\sum_{n=1}^{N}\left[\theta_t(n) - \theta_{f,j}(n)\right]^2}\,, \tag{13}$$

where $\theta(n)$ is n-th joint angle (for target or fiducial configuration) and N is the total number of robot joints. Then, the inverse distance $d_j' = 1/d_j$ was used to calculate the weight as

$$w_j = d_j'/\textstyle\sum_{j=1}^{J} d_j'\,. \tag{14}$$

IV. Verification

The performance of the extended RRBC procedure was investigated using both lab experiments with physical robots and computer simulations. The reduction in robot error was reported as a ratio ρ_{cor}/ρ_{unc} for orientation and $\delta_{cor}/\delta_{unc}$ for position error. Details of the experiment and simulations are provided below.

A. Case Study: Physical Experiments

A collaborative, open chain manipulator robot KUKA LWR 4+ was used in the experiments. According to the robot specification, the repeatability σ_{rep} of this 7DOF robot arm was ± 0.05 mm (ISO 9283). To ensure high accuracy in Cartesian space, the stiffness of the robot was set to high. In the tests, the third joint angle was fixed and set to zero. Thus, the effective number of joints was reduced to $N = 6$, and an in-house analytical inverse kinematic (AIK) module was used to solve the inverse kinematic problem rather than relying on the robot's built-in IK solver. Depending on the pose of the end-effector, the AIK module yielded up to eight unambiguous solutions.

A fixed, three-camera motion-capture system, an OptiTrack TRIO, was used as an external tracking system. Each of the three cameras has a resolution of 640×480 pixels, and the sampling frequency of the tracking system was set to 120 Hz. Four spherical infrared reflector (SIR) markers were attached to an aluminum plate mounted at the robot's tool flange, as shown in Fig. 1. These markers were used to get the 6DOF pose of the robot in the TRIO's coordinate frame. The tracking system output the location as (x, y, z) and three orientation angles $\left(\mu_x, \mu_y, \mu_z\right)$ parametrizing the Euclidean rotation matrix.

The robot was commanded to $K = 66$ different target poses. Around each target pose $(\mathbf{B}_k, \boldsymbol{\beta}_k)$, fiducial poses $\left(\boldsymbol{\Phi}_j, \boldsymbol{\varphi}_j\right)$ were defined so that the eight fiducial positions $\{\boldsymbol{\varphi}_1, \ldots, \boldsymbol{\varphi}_8\}$ were at the corners of a 20-mm cube with $\boldsymbol{\beta}_k$ at the center of the cube. At each of the eight cube corners, the same set of six orientations $\{\boldsymbol{\Phi}_1, \ldots, \boldsymbol{\Phi}_6\}$ was defined. If target orientation $\mathbf{B}_k$ was parametrized by angle ρ_k and axis $\boldsymbol{u}_k$, then three unit vectors $\{\boldsymbol{f}_1, \boldsymbol{f}_2, \boldsymbol{f}_3\}$ were selected in a way such that $\boldsymbol{u}_k$ was inside the spherical equilateral triangle formed by the three unit vectors, and the angular distance between $\boldsymbol{u}_k$ and each $\boldsymbol{f}$ was 7°. Two angles $\rho_k \pm 5°$ were selected as angles of rotation and

associated with each of the three unit vectors to parametrize the six fiducial orientation matrices. In this way, a total of $J = 48$ fiducial poses $(\boldsymbol{\Phi}_j, \boldsymbol{\varphi}_j)$ were built around each target pose $(\mathbf{B}_k, \boldsymbol{\beta}_k)$. This was repeated for all K targets resulting in a total of 3,168 fiducial poses. At each pose (target or fiducial), 12 repeated measurements were made with the TRIO system and stored in a file along with the joint angles corresponding to the commanded robot pose. In post-processing, the average pose, in the sensor frame, was calculated from the repeated measurements and used when analyzing the data.

From the set of all fiducial poses in the TRIO system frame and the robot frame, eight pairs of poses were randomly selected and used to obtain the hand-eye calibration matrices $(\widehat{\boldsymbol{X}}, \widehat{\boldsymbol{Y}})$ as in [39].

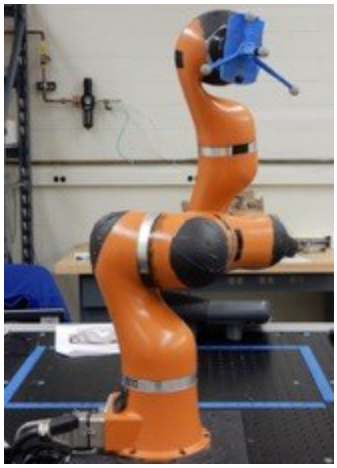

Fig. 1. Four spherical, reflective markers used to track the pose at the end of a robot arm.

B. Case Study: Computer Simulation

In the computer simulation, the commanded robot poses were calculated using joint angles obtained from both the lab experimentation and the forward kinematic model with the same set of parameters as used by the robot controller. Then, using the inverse hand-eye transformation $(\widehat{\boldsymbol{X}}^{-1}, \widehat{\boldsymbol{Y}}^{-1})$ obtained from the experimental data, corresponding poses in the sensor frame were generated. Finally, joint angle offsets were slightly deviated from their nominal values used in the experiment and new, "erroneous" commanded poses in robot frame were generated using the same set of joint angles as before. Once the two sets of corresponding poses in robot and sensor frame were created, the rest of the post-processing was the same as for the experimental data, i.e., quantities defined in equations (8) through (14) were calculated.

V. Results

From the 12 repeated TRIO measurements of positions and orientation angles, sensor noise was calculated as the standard deviation at each measured pose, and then the average over all poses in the work volume was estimated yielding $\bar{\sigma}_{pos} \approx 0.057$ mm for the position component and $\bar{\sigma}_{ang} \approx 0.06°$ for the angular component. Deviation from the rigid-body assumption was investigated by calculating the differences in relative rotations between the k-th target and its surrounding 48 fiducials when determined in both the robot and sensor frames. The histogram of such differences $\Delta_{k,j} = \rho_{k,j}^{sen} - \rho_{k,j}^{rob}$ is shown in Fig. 2, where

$$\boldsymbol{R}(\rho_{k,j}^{sen}, \boldsymbol{u}_{k,j}^{sen}) = \boldsymbol{\Phi}_j \, \mathbf{B}_k^T \,, \tag{15}$$

and $\boldsymbol{R}$ is the relative rotation between the k-th target orientation $\mathbf{B}_k$ and the associated j-th fiducial orientation $\boldsymbol{\Phi}_j$ in the sensor frame. The corresponding relative rotation $\boldsymbol{R}(\rho_{k,j}^{rob}, \boldsymbol{u}_{k,j}^{rob})$ was also calculated in the robot frame so that the differences $\Delta_{k,j}$ could be calculated for all j and k. Note that the calculations of the differences do not require hand-eye registration, and the deviation from the rigid-body condition may be characterized by a single parameter (e.g., the standard deviation of differences σ_Δ). For the experimental data shown in Fig. 2, $\sigma_\Delta = 0.405°$ and roughly 25% of this value may be attributed to sensor inaccuracy and the remaining part to the uncalibrated robot.

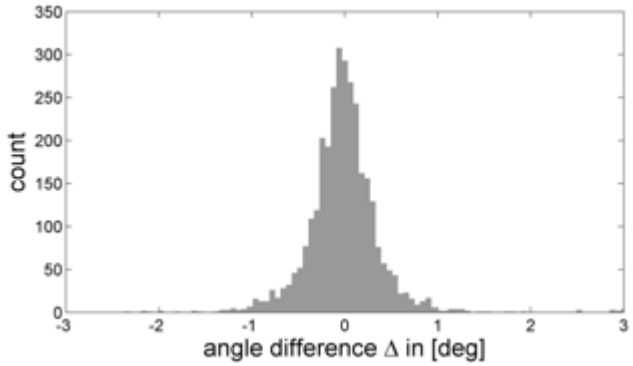

Fig. 2. Histogram of angular differences which result from deviation from the rigid-body condition for the robot-sensor system.

The uncorrected $(\rho_{unc}, \delta_{unc})$ and corrected $(\rho_{cor}, \delta_{cor})$ target errors defined in (11) and (12) are shown in Fig. 3 and Fig. 4 for the experimental data, and in Fig. 5 and Fig. 6, for the simulated data, respectively. The median (from $K = 66$) values of the errors $(\hat{\delta}, \hat{\rho})$ and corresponding reduction rates $(\gamma_{pos}, \gamma_{ang})$, where $\gamma_{pos} = (\hat{\delta}_{unc} - \hat{\delta}_{cor})/\hat{\delta}_{unc}$ and $\gamma_{ang} = (\hat{\rho}_{unc} - \hat{\rho}_{cor})/\hat{\rho}_{unc}$, are given in Table I.

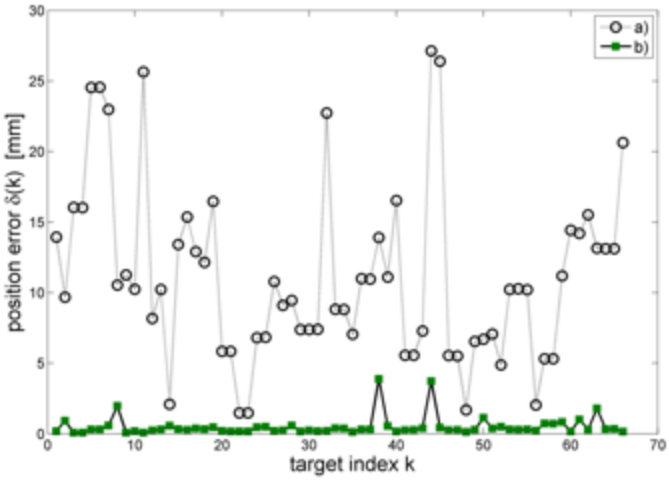

Fig. 3. Robot position error from experimental data: a) uncorrected error δ_{unc}; b) corrected error δ_{cor}.

For the k-th target and its corresponding robot joint angles $\boldsymbol{\theta}_t$, all distances d_j in (13) are calculated for $j = 1, \ldots, 48$. The largest d_j is denoted by $\theta_{max}(k)$ and plotted for all K targets in Fig. 7.

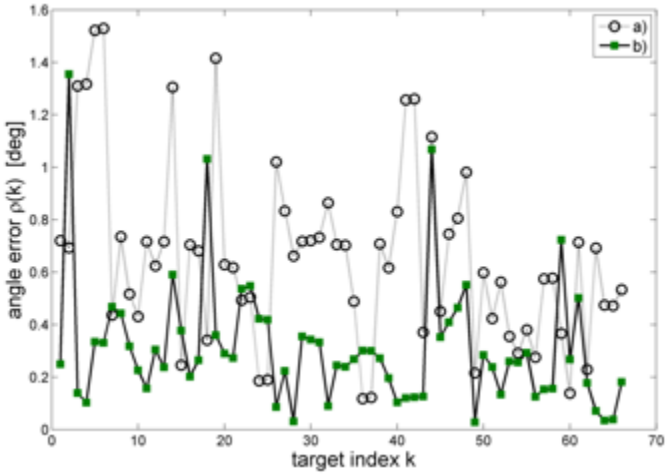

Fig. 4. Robot orientation error from experimental data: a) uncorrected error ρ_{unc}; b) corrected error ρ_{cor}.

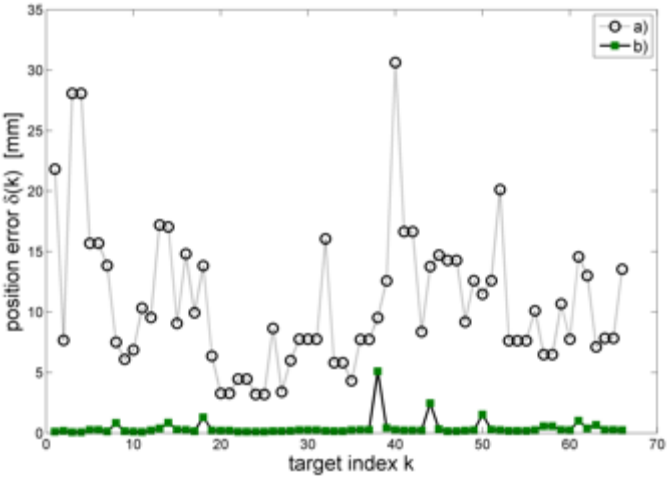

Fig. 5. Robot position error from simulated data: a) uncorrected error δ_{unc}; b) corrected error δ_{cor}.

Table I. Median robot errors

Data source	Median position error [mm]			Median angle error [deg]		
	$\hat{\delta}_{unc}$	$\hat{\delta}_{cor}$	γ_{pos}	$\hat{\rho}_{unc}$	$\hat{\rho}_{cor}$	γ_{ang}
Exp.	10.233	0.301	97 %	0.626	0.267	57 %
Sim.	9.128	0.228	97 %	0.952	0.010	99 %

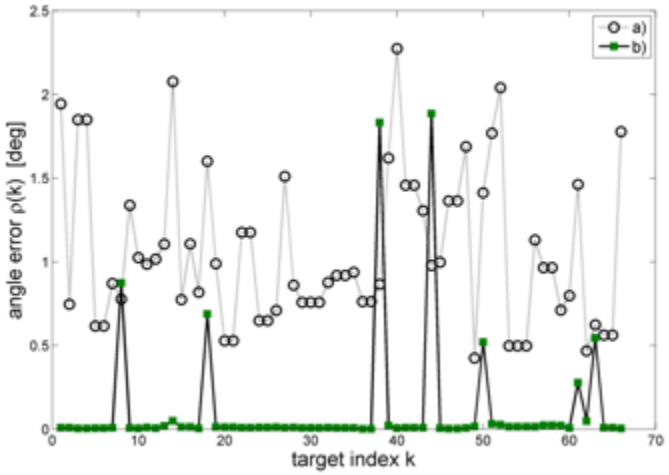

Fig. 6. Robot orientation error from simulated data: a) uncorrected error ρ_{unc}; b) corrected error ρ_{cor}.

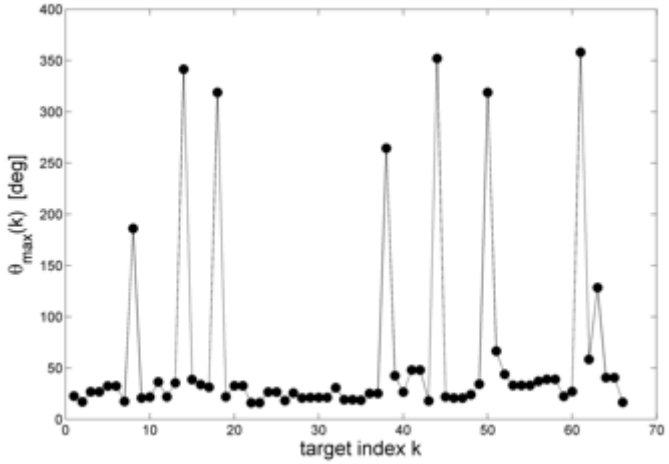

Fig. 7. Largest angle distance between joint angles at a target and the commanded poses for its neighboring fiducials.

VI. Disussion

The presented results show that pose accuracy of a robot's end-effector can be greatly improved. Both position and orientation errors can be reduced by linear interpolation of small corrections (small rotations and small translations) obtained from neighboring fiducial poses for which the rigid-body condition has been restored. In the lab experiments, the observed improvement in the position is larger than in the orientation. Plots in Fig. 3 show that for all K targets, the corrected position error $\delta_{cor}(k)$ is smaller than the uncorrected error $\delta_{unc}(k)$. For the orientation error (Fig. 4), the RRBC method failed for 11 out of 66 targets (i.e., when $\rho_{cor}(k)$ is larger than uncorrected $\rho_{unc}(k)$). This outcome is not unexpected as the method relies on linear interpolation which may occasionally give inaccurate estimates, especially when the distance between target and fiducial is not small. However, the same procedure was also used to process the simulated data (which were generated using the recorded experimental joint angles), and it led to failure for

only three target orientations, as can be seen in Fig. 6. To explain the difference between the experimental and simulated results (as evidenced by numerical values of $\hat{\rho}_{cor}$ and γ_{ang} in Table I), a more detailed analysis of differences between experimental and simulated data is needed. For both experimental and simulated trials, the RRBC method resulted in a net increase in position accuracy.

Each target pose was surrounded by 48 fiducial poses, methodically designed for linear interpolation: six orientations at each of the eight cube corners. At each of the eight corners, the same set of six different, commanded orientations was used. Therefore, for each orientation, there were eight repeats, and this enabled the evaluation of the variance of the angles (μ_x, μ_y, μ_z) measured by the TRIO. The three variances were summed up, and the same calculations were repeated for all six orientations. The mean variance was then evaluated, and its square root was used as the mean variation for that target, $g(k)$. These calculations were performed for each target, and the results are shown in Fig. 8. Since each of the 48 fiducial poses is a combination of one orientation and one position, each pose corresponds to a unique arm configuration. Because no calibration is perfect, the robot is expected to have some residual calibration error. As such, each of the six orientations at all eight cube corners is expected to demonstrate some variability across measurements by the TRIO. However, the variability seen in Fig. 8 cannot be attributed to a random noise; recall that all post-processing was performed on the averaged TRIO data.

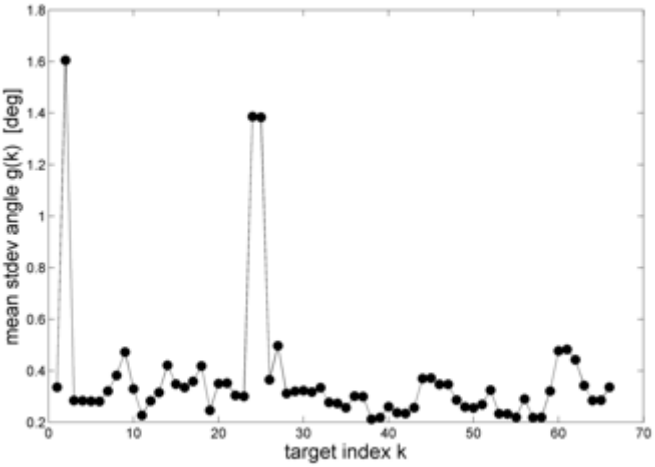

Fig. 8. Variations of measured by sensor angles corresponding to fixed commanded orientations in robot frame.

This variability also impacts the orientation correction $\boldsymbol{\Lambda}_j$ in (8a). For a commanded orientation $\boldsymbol{A}_j$ in the robot frame, the orientation $\boldsymbol{B}_j$ measured by TRIO depends on the commanded position $\boldsymbol{a}_j$ although in (8a) the positional component of the pose is not explicitly used. Thus, the orientation $\boldsymbol{B}_j$ can be expressed as some constant orientation $\overline{\boldsymbol{B}}_j$ perturbed by a small rotation matrix $\boldsymbol{dR}_j$ which depends on $\boldsymbol{a}_j$, i.e., $\boldsymbol{B}_j = \boldsymbol{dR}_j(\boldsymbol{a}_j)\,\overline{\boldsymbol{B}}_j$. Although the root cause of the small perturbation $\boldsymbol{dR}_j$ is purely deterministic (uncalibrated robot), its effect on the linear interpolation scheme is similar to random noise: it makes the correction $\boldsymbol{\Lambda}_j$ ambiguous and less accurate. This affects the estimated target correction in (9a) and lessens the reduction of the orientation error ρ_{cor} in (12a). This phenomenon is not present in the simulated data because rotations in the sensor frame were created from the commanded robot rotations using the inverse hand-eye transformation $(\widehat{\boldsymbol{X}}^{-1}, \widehat{\boldsymbol{Y}}^{-1})$. Note that the position correction $\boldsymbol{\lambda}_j$ in (8b) depends explicitly on the commanded pose $(\boldsymbol{A}_j, \boldsymbol{a}_j)$, and therefore, it can be uniquely determined. This explains why the reduction in the position error γ_{pos} for the experimental data is as good as for the simulated data (as shown in Table I).

Closer inspection of the target poses for which the reduction procedure underperformed (i.e., the corrected robot errors are conspicuously larger) reveals a strong correlation with targets where $\theta_{max}(k)$ spikes over $100°$. This is observed for the position and orientation error and for both types of data: experimental and simulated, as can be seen by comparing Fig. 7 with Fig. 3 through Fig. 6. Although the Euclidean and angular distances between the target and fiducial are small, large differences between two robot arm configurations will degrade the performance of the linear interpolation technique. No correlation between large $\theta_{max}(k)$ and the location of the k-th target in the work volume was observed. Note that the three target poses characterized by large variation $g(k)$, as shown in Fig. 8, also coincide with the locations where the reduction of the orientation error failed, i.e., $\rho_{cor}(k) > \rho_{unc}(k)$. Whether this large variation $g(k)$ is caused entirely by the sensitivity of the orientation correction $\boldsymbol{\Lambda}_j$ (8a) to the position $\boldsymbol{a}_j$ (i.e., large rotation perturbation $\boldsymbol{dR}_j(\boldsymbol{a}_j)$) or by a deficiency in the data acquired by the sensor needs to be investigated. When 11 poses with large $\theta_{max}(k)$ or $g(k)$ are discarded, the median errors from the remaining 55 target poses are reduced to $\hat{\delta}_{cor} = 0.279$ mm for position and $\hat{\rho}_{cor} = 0.249°$ for orientation.

VII. Conclusions

Unlike most other error compensation techniques which reduce only position error, the extended Restoration of Rigid Body Condition method also reduced the orientation error of a robot's end-effector. That was demonstrated on experimental data requiring hand-eye calibration. Performance of the method can be improved by choosing fiducial arm configurations that are close to the target arm configuration. The relative reduction of the orientation error was smaller than for position error. This is a consequence of the mathematical property of the hand-eye calibration, and the fact that target corrections were estimated in Cartesian space. Estimating these corrections in joint angle space could overcome the limits of the existing method and is planned for future research.

Disclaimer

Certain commercial equipment are mentioned in this paper to specify the experimental procedure adequately. Such identification is not intended to imply recommendation or endorsement by the National Institute of Standards and Technology, nor does it imply that the equipment is necessarily the best available for the purpose.

REFERENCES

[1] B. Greenway, "Robot Accuracy," *Industrial Robot: An International Journal,* vol. 27, no. 4, pp. 257-265, 2000.

[2] M. Slamani, A. Nubiola, and I. A. Bonev, "Assessment of the Positioning Performance of an Industrial Robot," *Industrial Robot,* vol. 39, no. 1, pp. 57-68, 2012.

[3] R. Usubamatov, S. A. Adam, and A. Harun, "Analyzing the jamming of parts on the shaft in assembly processes," *Assembly Automation,* vol. 32, no. 4, pp. 340-346, 2012.

[4] W.Zhu, W.Qu, L.Cao, D.Yang, and Y.Ke, "An off-line programming system for robotic drilling in aerospace manufacturing," *Int. J. Advanced Manufacturing Technology,* vol. 68, pp. 2535–2545, 2013.

[5] L.Tingelstad, A.Capellan, T.Thomessen, and T.K.Lien, "Multi-Robot Assembly of High-Performance Aerospace Components," presented at the 10th IFAC Symposium on Robot Control, Dubrovnik, Croatia, 2012.

[6] F. Franceschini, M. Galetto, D. Maisano, and L. Mastrogiacomo, "Large-scale dimensional metrology (LSDM): from tapes and theodolites to multi-sensor systems," *Int. J. Precision Engineering and Manufacturing,* vol. 15, no. 8, pp. 1739 - 1758, 2014.

[7] H. P. Stahl, "Metrology of Large Parts," in *Handbook of Optical Dimensional Metrology*, K. Harding, Ed.: CRC Press, 2012, pp. 239 - 262.

[8] J. Ross, K. Harding, and E. Hogarth, "Challenges faced in applying 3D noncontact metrology to turbine engine blade inspection," in *Proc. SPIE Dimensional Optical Metrology and Inspection for Practical Applications*, San Diego, CA, 2011, vol. 8133, pp. 81330H-1 - 81330H-9.

[9] C. Liu, Y. Li, and X. Hao, "An adaptive machining approach based on in-process inspection of interim machining states for large-scaled and thin-walled complex parts," *Int. J. Advanced Manufacturing Technology,* vol. 90, pp. 3119-3128, 2017.

[10] R. Judd and A. Knasinski, "A technique to calibrate industrial robots with experimental verification," *IEEE Trans. Robotics and Automation,* vol. 6, no. 1, pp. 590-596, 1990.

[11] K. Conrad, P. Shiakolas, and T. Yih, "Robot Calibration Issues: Accuracy, Repeatibility and Calibration," in *8th Medit. Conf. Control and Automation*, Rio Patras, Greece, 2000.

[12] S. Aoyagi, A. Kohama, Y. Nakata, Y. Hayano, and M. Suzuki, "Improvement of Robot Accuracy by Calibrating Kinematic Model Using a Laser Tracking System - Compensation of Non-Geometric Errors Using Neural Networks and Selection of Optimal Measuring Points Using Genetic Algorithm," presented at the IEEE/RSJ Int. Conf. on Itelligent Robots and Systems, Taipei, Taiwan, 2010.

[13] J. Santolaria, J. Conte, and M. Gines, "Laser tracker-based kinematic parameter calibration of industrial robots by improved CPA method and active retroreflector," *Int. J. Advanced Manufacturing Technology,* vol. 66, pp. 2087 - 2106, 2013.

[14] Y. Wu, A. Klimchik, S. Caro, B. Furet, and A. Pashkevich, "Geometric calibration of industrial robots using enhanced partial pose measurements and design of experiments," *Robotics and Computer-Integrated Manufacturing,* vol. 35, pp. 151 - 168, 2015.

[15] F. Chaumette and S. Hutchinson, "Visual Servo Control Part I: Basic approaches," *IEEE Robotics and Automation Magazine,* vol. 13, no. 4, pp. 82-90, 2006.

[16] F. Chaumette and S. Hutchinson, "Visual Servo Control Part II: Advanced Approaches," *IEEE Robotics and Automation Magazine,* vol. 14, no. 1, pp. 109 - 118, 2007.

[17] J.Bos, A.Wahrburg, and K.D.Listmann, "Iteratively Learned and Temporally Scaled Force Control with Application to Robotic Assembly in Unstructured Environments," presented at the IEEE Int. Conf. on Robotics and Automation (ICRA), Singapore, 2017.

[18] Z. Liu, Y. Xie, J. Xu, and K. Chen, "Laser tracker based robotic assembly system for large scale peg-hole parts," presented at the Int. Conference on Cyber Technology in Automation, Control and Intelligent Systems, Hong Kong, China, 2014.

[19] K. V. Wyk, M.Culleton, J.Falco, and K.Kelly, "Comparative Peg-in-Hole Testing of a Force-based Manipulation Controlled Robotic Hand," *IEEE Trans. on Robotics,* 2018.

[20] Y.Xu, Y.Hu, and L.Hu, "Precision Peg-in-Hole Assembly Strategy Using Force-Guided Robot," presented at the 3rd Int. Conf. on Machinery, Materials and Information Technology Applications (ICMMITA), Qingdao, China, 2015.

[21] E. Kiraci, P. Franciosa, G. A. Turley, A. Olifent, A. Attridge, and M. A. Williams, "Moving towards in-line metrology: evaluation of a Laser Radar system for in-line dimensional inspection for automotive assembly systems," *Int. J. Advanced Manufacturing Technology,* vol. 91, pp. 69 - 78, 2017.

[22] C. Mineo, S. G. Pierce, B. Wright, I. Cooper, and P. I. Nicholson, "PAUT inspection of complex-shaped composite materials through six DOFs robotic manipulators," *Insight - Non-Destructive Testing and Condition Monitoring,* vol. 57, no. 3, pp. 161-166, 2015.

[23] A. Angelidis and G.-C. Vosniakos, "Prediction and compensation of relative position error along industrial robot end-effector paths," *Int. J. Precision Engineering and Manufacturing,* vol. 15, no. 1, pp. 63-73, 2014.

[24] B.Muralikrishnan *et al.*, "Volumetric performance evaluation of a laser scanner based on geometric error model " *Precision Engineering,* vol. 40, pp. 139-150, 2015.

[25] D. A. Bristow, M. Tharayil, and A. G. Alleyne, "A Survey of Iterative Learning Control," *IEEE Control Systems Magazine,* vol. June pp. 96-114, 2006.

[26] C. Cajal, J. Santolaria, D. Samper, and J. Velazquez, "Efficient volumetric error compensation technique for additive manufacturing machines," *Rapid Prototyping Journal,* vol. 22, no. 1, pp. 2 - 19, 2016.

[27] M. Galetto, L. Mastrogiacomo, G. Moroni, and S. Petrò, "Volumetric Error Compensation for the MScMS-II," in *12th CIRP Conference on Computer Aided Tolerancing*, 2013, pp. 98 - 104: Elsevier.

[28] S. K. Mustafa, P. Y. Tao, G. Yang, and I.-M. Chen, "A Geometrical Approach for Online Error Compensation of Industrial Manipulators," presented at the IEEE/ASME Int. Conf. on Advanced Intelligent Mechatronics, Montreal, Canada, 2010.

[29] P. Y. Tao, G. Yang, and M. Tomizuka, "A Sensor-based Approach for Error Compensation of Industrial Robotic Workcells," presented at the IEEE Int. Conf. on Robotics and Automation IROS, Saint Paul, MN, 2012.

[30] K. S. Arun, T. S. Huang, and S. D. Blostein, "Least-Squares Fitting of Two 3-D Point Sets," *IEEE Trans. PAMI,* vol. 9, no. 5, pp. 698-700, 1987.

[31] M. Franaszek, G. S. Cheok, K. v. Wyk, and J. A. Marvel, "Improving 3D Vision-Robot Registration for Assembly Tasks," *unpublished*.

[32] H. Zuang, Z. Roth, and R. Sudhakar, "Simultaneous robot/world and tool/flange calibration by solving homogeneous transformation equations of the form ax=yb," *IEEE Trans. Robotics and Automation,* vol. 10, no. 4, pp. 549-554, 1994.

[33] D. E. Myers, "Spatial interpolation: an overview," *Geoderma,* vol. 62, pp. 17-28, 1994.

[34] D.Chen, P.Yuan, T.Wang, and C.Ying, "A compensation method based on error similarity and error correlation to enhance the position accuracy of an aviation drilling robot," *Meas. Sci. Technol.,* vol. 29, pp. 1-11, 2018.

[35] Y. Zeng, W. Tian, D. Li, X. He, and W. Liao, "An error-similarity-based robot positional accuracy improvement method for a robotic drilling and riveting system," *Int. J. Advanced Manufacturing Technology,* vol. 88, pp. 2745 - 2755, 2017.

[36] R. A. Olea, "A six-step practical approach to semivariogram modeling," *Stochastic Environmental Research and Risk Assessment,* vol. 20, no. 5, pp. 307-318, July 01 2006.

[37] Y. Bai, "On the comparison of model-based and modeless robotic calibration based on a fuzzy interpolation method," *Int. J. Advanced Manufacturing Technology,* vol. 31, pp. 1243 - 1250, 2007.

[38] Y. Bai and D. Wang, "On the Comparison of Trilinear, Cubic Spline, and Fuzzy Interpolation Methods in the High-Accuracy Measurements," *IEEE Trans. Fuzzy Systems,* vol. 18, no. 5, pp. 1016 - 1022, 2010.

[39] M. Shah, "Solving the Robot-World/Hand-Eye Calibration Problem using the Kronecker Product," *J. Mechanisms and Robotics,* vol. 5, no. 3, pp. 031007-031007-7, 2013.

[40] M. Moakher, "Means and Averaging in the Group of Rotations," *SIAM J.Matrix Analysis and Applications,* vol. 24, no. 1, pp. 1-16, 2002.